EXPERIMENTAL AND NUMERICAL STUDY OF RHOMBOIDAL MIXING SECTIONS

Antoine C. Rios[•]*, Paul J. Gramann*[•] *and Tim A. Osswald*
Polymer Processing Research Group
Department of Mechanical Engineering
University of Wisconsin-Madison
Madison, Wisconsin 53706
Maria del P. Noriega and Omar A. Estrada
Instituto de Capacitación e Investigación del Plástico y del Caucho (ICIPC)
Medellín, Colombia

Abstract

The rhomboidal mixing section is becoming very popular among processors to provide distributive mixing. Currently, several different designs are used but the details of the flow behavior and mixing efficiency is not well understood. This information is needed to be able to design and find the most efficient rhomboid geometry. In this investigation nine different geometries with various pitches (helix of rhomboids) were analyzed using a 3-dimensional boundary element method (BEM). The geometries were compared according to mixing efficiency, pressure and energy consumption. The results were compared to experiments performed with a conventional single screw extruder that was fitted with three different rhomboidal mixing sections. The investigation led to the conclusion that the most effective distributive mixing sections were those with neutral rhomboids (pineapple mixer). However, the neutral rhomboidal mixing section consumes the most pressure in the extruder. It was also concluded that rhomboidal mixing sections deform the material by shear, making them poor dispersive mixing sections.

1 Introduction

Mixer design is slowly changing from being a complete experimental process to a partially numerical and experimental one. Numerical simulation has an advantage that analysis and optimization can be performed before the device is built. Consequently, the design of new mixing devices becomes less expensive and at the same time faster.

The rhomboidal mixing section is becoming a standard for improving mixing during extrusion. This mixing device can have numerous configurations depending on the number and pitch of helical cuts. Figure 1 shows the helical cuts and other parameters used in the rhomboid construction. The performance of the rhomboidal mixing section depends completely on the type of configuration to be used. Therefore, a comparison of various designs is desired in order to obtain the most efficient geometry.

Several researchers have performed experiments with rhomboidal mixing sections [1-3]. These studies used various rhomboidal designs, and for all cases an improvement in mixing was observed when compared to a conventional single screw extruder with no mixing section. Other studies [4-6] used a numerical approach for analyzing the flow inside a rhomboidal mixer, but without performing any comparison.

• Present address: The Madison Group, 505 S. Rosa Rd., Madison, WI 53719

The mixing action that takes place in polymer processing can be broken down into two major categories—distributive mixing and dispersive mixing. The first exists when the homogenization of a secondary phase within the matrix is desired, and the latter, when the breaking of the secondary phase into smaller particles is desired. The mixing phenomena highly depends on the material behavior during the process. For distributive mixing, high strains are required in order to increase the interfacial area between the two or more phases and reduce the striation thickness of the secondary phase. For dispersive mixing the presence of high stresses, which is dependent on the rate of strain, is more important.

This research presents, for the first time, a comparative study of different rhomboidal mixing sections. The results shown here help to understand how design changes of the mixing sections influence the various mixing mechanism required for distribution and dispersion during polymer processing. A numerical analysis of nine different rhomboid mixing sections, each having a different pitch, is presented here. Figure 2 shows the geometries used and Table 1 lists the main specifications of each rhomboidal section. For the study, a 3-dimensional, Newtonian flow simulation program using the boundary element method (BEM) was used to solve the flow field of each rhomboidal mixing section. For each case, after the flow field was calculated, the mixer efficiency was assessed. The efficiency was measured and compared by analyzing the mixing performance along with pressure and energy consumption for each of the nine geometries. The numerical results of three rhomboids were compared to experiments performed with a conventional screw fitted with identical rhomboids. Experimental results were obtained with the same extruder, processing conditions and material. The comparison involves the analysis of the characteristic curves, temperature homogenization and mixing capability of each configuration.

2 Numerical Analysis

Traditionally, simulation of polymer processing equipment is accomplished by using numerical simulation that involves domain discretization with finite differences, finite volumes or finite elements [7-11]. The use of a discrete domain involves the complex generation of a 3-dimensional mesh. This can be a time consuming step and requires a great deal of computational power. BEM eliminates the need of domain discretization and requires only the use of discrete boundaries, reducing the mesh generation step to the creation of two-dimensional shell elements instead of creating 3-dimensional volume elements. Because processing equipment is generally composed of complex geometries, the shell mesh is faster and easier to generate, which greatly reduces the effort of simulation set-up. Furthermore, when simulating processing equipment with rotating elements, the mesh remains constant and does not need to be updated each time step. Conventional domain techniques require the generation of a new mesh as the boundaries rotate.

The geometries used in this study generally consisted of between 1000 and 1400 quadratic shell elements and between 3000 and 5000 nodes. For the mixing analysis, 200 particles were randomly located at the beginning of the mixing section and tracked until they exited the mixer. The particles were tracked using the Crank-Nicolson method. All calculations were completed on a desktop computer; a SGI Indigo2 R10000 with 384 MB of RAM. The solution of the large matrices obtained with the boundary element simulation was accomplished by an out of core solver [12], which solves the matrix by dividing it in blocks that fit in the internal RAM of the machine (in core) and saving the rest to a hard drive. The time required to solve for the unknowns was approximately 4 hours. Time for particle tracking highly depends on the time step and was approximately 20 hours.

To model the flow and pressure fields a Newtonian fluid is considered. Further, during mixing of most polymers the Reynolds' number is much smaller than one, and the inertia effects can be neglected. Viscous heating effects are dropped when assuming an isothermal process. These assumptions are valid

when qualitatively analyzing the mixer, where the general tendencies of mixing are important rather than the fine details of the flow.

After neglecting the compressibility of the polymer, the continuity equation reduces to

$$\nabla \cdot \underline{U} = 0 \quad . \tag{1}$$

Considering the assumptions mentioned earlier, the momentum balance simplifies to:

$$-\nabla P + \mu \nabla^2 \underline{U} = 0 \quad . \tag{2}$$

These equations cannot be solved analytically for the complicated geometries commonly found in polymer processing equipment. Here, to solve these equations numerically, the boundary element method was used. Several researchers have successfully utilized BEM [13-17]. With BEM, the dispersive and distributive mixing effect, streamlines, pressures, residence time distributions and torque can be calculated.

The derivation of Eqns. (1) and (2) into boundary integrals is shown in Gramann [17] and is based on work done by Lorenz [18] and Ladyzhenskaya [19]. The resulting boundary integral equation for Newtonian, isothermal, incompressible creeping flow is

$$C_i U_\kappa^i + \int_\Gamma \left[t_\alpha^\kappa U_\alpha - t_\alpha U_\alpha^\kappa \right] d\Gamma = 0 \tag{3}$$

where *i* is a point where the velocity is being solved for and C_i depends on the location of point i: C_i=1.0 inside the domain, C_i=0.0 outside the domain, or, C_i=0.5 on the boundary. t_α^κ and U_α^κ are the fundamental solutions for tractions and velocities in the α direction at the field point i caused by concentrated forces acting in the κ directions at the source point. Equation (3) contains only boundary integrals and fully satisfies the governing equations. Thus, it can be solved numerically by discretizing the boundary of the problem. Once the unknowns on the boundary are solved for, Eq. (3) can be used to solve for velocity at any point inside the domain.

To measure the efficiency of each rhomboidal mixing section the boundary conditions are non-dimensionalized. The pressure difference through the mixing sections is adjusted to maintain the same throughput for all sections.

2.1 Distributive Mixing Analysis

Distributive mixing is dependent on the amount of strain imposed on the material. The total strain that the material has undergone at time, *t'*, can generally be described by

$$\gamma(t') = \int_0^{t'} \dot{\gamma}(t) dt \tag{4}$$

where, $\dot{\gamma}(t)$ is the magnitude of the strain rate tensor. Generally, it is desired to impose as large a strain as possible to generate the most effective mixing. However, this does not take into account initial conditions and material reorientations [20], which enhance distributive mixing.

The shape of the cumulative residence time distribution (CRTD) can also be a useful measure of mixing, but only for mixing in the axial direction [21]. The extreme cases of the CRTD are plug flow and perfect mixing. In plug flow all the material moves together and has the same residence time represented as a vertical line. Perfect mixing exhibits a broad distribution where the material is

instantaneously and completely mixed in the system. Perfect mixing exists in a continuous stirred tank with constant discharge. A real system always falls between these ideal cases. To measure the efficiency of the real system with respect to a plug flow or a perfect mixer, Bigg [21] proposed a mixing index, β, that relates the two ideal curves and the actual measured curve. For a perfect mixer β equals 1.0, and 0.0 for plug flow.

2.2 Dispersive Mixing Analysis

Dispersion can be assessed by considering the type of flow and the stress, which is proportional to the strain rate that the material undergoes. When elongational flow is present, the maximum forces trying to disperse the secondary phase is over twice as large as those present in shear flow [22], making elongational flow preferred over shear flow for dispersive mixing. To evaluate the type of flow, several researchers have used the flow number [9, 13-17], which is defined as

$$\lambda = \frac{|\dot{\gamma}|}{|\dot{\gamma}| + |\omega|} \tag{5}$$

where $|\dot{\gamma}|$ and $|\omega|$ are the magnitude of the strain rate and vorticity tensors, respectively. The flow number is a non-dimensional quantity that ranges from 0.0 for pure rotational flow to 1.0 for pure elongational flow with 0.5 denoting shear flow. In practical applications a purely elongational flow (λ =1) is not possible. However, when designing for dispersive mixing the goal is to obtain a flow number near 1.0 and at the same time maintain high stresses.

2.3 Characteristic Curves

The characteristic or operation curve shows the behavior of the mixing section by relating flow rates and pressure differences between the inlet and outlet of the section. The pressure difference is an important measure since it defines the size of various components on the extruder. A mixing section consuming higher pressure requires a screw that can build-up more pressure in order to keep the flow rate unchanged. In this paper the flow rates were calculated by integrating the velocity of the material across the outlet side of each mixer.

The torque required to turn the screw at a specified flow rate is important for calculating the efficiency of the mixer. Torque is calculated by integrating the resulting tractions on the boundary elements. Torque is also a factor that defines the size of the motor and screw of the extruder. In general, an efficient and economical extruder is characterized by its low torque and pressure consumption.

3 Experimental Analysis

The experiments for this study were performed on a highly instrumented Extrudex ED-N-45-25D single screw extruder located at the Plastics Institute (ICIPC) in Medellin, Colombia. The extruder was equipped with a conventional 45 mm three zone screw (8D/11D/4D+2D) with a 2.33:1 compression ratio. The screw has a threaded end such that various mixing sections can be attached. Figure 3 shows a picture of each mixing device, which have the same specifications as the corresponding rhomboids described in the numerical results on Table 1. The material used for the experiments was a high density polyethylene (HDPE – Altaven 620) with a power law index of n=0.41 and a consistency index of m=16624 $Pa \cdot s^n$ at 210 °C.

The trials were conducted under the same heating band temperature profile (160, 170, 180, 190, 200 °C) with three different die openings and three screw speeds for a total of nine operating points per

trial. The performance of each mixer was evaluated by means of the characteristic curve. To measure the screw characteristic curves the extruder is fitted with a pressure transducer located before the die. The mass flowrate is measured by weighing the amount of material exiting the extruder in a 30 seconds interval.

Mixing performance was assessed by subjective comparison of micrographs taken from a cross-section of the extrudate. The extrudate was a mix of a yellow master batch pigment with the respective polymer. The mixing by thermal homogeneity was measured by the melt temperature profile. The profile was measured with a five sensor thermal comb located 2D after the end of the screw.

Depending on the type of rhomboid mixer utilized in the screw, the operating range of the extruder differed. The extruder performance is not only controlled by the mixer, but is dependent on the combination of the screw design from the hopper to the die. The screw characteristic curves shown in Fig. 4 reveal the extruder's (screw + mixer) operation range. For simplicity, these curves were non-dimensionalized using the measured rheology of HDPE and the dimensions of the screw as,

$$m^* = \frac{m_f}{\rho N D^3} \tag{6}$$

and

$$\Delta p^* = \frac{\Delta p D}{m N^n L} \tag{7}$$

where m_f is the mass flowrate, ρ the material density (950 Kg/m^3), N the screw rotational speed, D the diameter of the screw, Δp the pressure drop at the die, n and m are the power-law and consistency index of the material and L is the length of the screw.

4 Results and Discussion

4.1 Characteristic Curves

Figure 5 shows the numerical calculated characteristic curves of the nine rhomboids. The data on the positive side of the chart represents a mixing device that produces pressure and the negative side a device that consumes pressure. From these figures it is seen that the rhomboid 1D4D is the mixing device with more pumping capability, while the pineapple 1.6D (rhomboid –1.6D1.6D) is the highest pressure consumer. This can be explained by looking at Fig. 2. Here, the rhomboid 1D4D looks more like a single screw extruder, which is a net pressure producing device. The pineapple 1.6D has the most restrictions or rhomboids through which the material has to flow around causing a bigger pressure loss. As the mixing sections have more obstructions to the flow, i.e. more rhomboids per area, the pressure losses increase. Figure 5 shows that the flowrate is zero for the two pineapple mixers (rhomboid –2D2D and rhomboid –1.6D1.6D) when the pressure difference is zero. This neutral effect is caused by the two counter helixes present in the pineapple mixers. One helix pumps material forward while the other pumps backwards.

Analyzing the experimental characteristic curves in Fig. 4, for the operation range tested, the pineapple 1.6D gave the lowest output characteristics compared to the other mixers. Each point on Fig. 4 represents the mean of the non-dimensional operating points for three screw speeds. The error bars shown are for a 90% confidence interval and 6 experimental measurements (2 samples per screw speed). Due to the viscous heating created with more restrictive dies the material temperature increases. Since the non-dimensionalization is isothermal, it does not take into account the temperature changes

leading to a larger error at high pressures. This finding is in agreement with the numerical results where the pineapple 1.6D was found to be a higher pressure consumer.

4.2 Residence Time Distribution

The residence time distribution can be calculated numerically by tracking particles and measuring the time that each particle spends in the extruder or mixing device. The cumulative residence time distributions (CRTD) is computed by integrating the residence time distribution. The CRTD for the rhomboidal mixing sections are shown in Fig. 6. Here, only five curves (rhomboids 1D3D, 2D4D, -1D6D and pineapples 2D and 1.6D) are displayed. The other four (rhomboids 1D2D, 1D3D, 1D4D and 1D6D), which are not shown for clarity, have CRTD curves very similar to those of the rhomboids 1D3D and 2D4D.

The last column of Table 2 shows the calculated parameter β for the rhomboids. It is shown that the two pineapple mixers show the highest similarity to a perfect mixer with a value of approximately 0.5. The rhomboid with the negative pitch (-1D6D) comes second with β=0.33. The three rhomboids with one negative pitch are more restrictive for the material resulting in a broader RTD. However, for materials sensitive to degradation these mixers are not recommended due to the higher residence time of the material. Rhomboid 1D3D presents the worst axial mixing according to RTD with β=0.15. The rest of the rhomboids have very similar RTD with β approximately 0.25. This result shows that the pineapple mixers have the best mixing capability in the main flow direction. In this section, as the material splits around the rhomboid, it can be transported back axially. Whereas when splitting occurs in the other rhomboids all material pumps forward giving a lower residence time.

For all the rhomboids there is a good correlation between the mean residence time, total strain and the β parameter. As the material stays longer in the mixer more strain is imposed and the RTD tends to be broader (higher β).

4.3 Mixing Analysis

Table 2 shows the numerical results of the rhomboidal mixing sections mean residence time ($\bar{t}$), mean total strain, mean flow number and mean strain rate. These quantities are obtained from the history of the 200 particles tracked through the sections. It is known that the initial position of the particles has an effect on the results. The variance on the final results is decreased as the number of tracking particles increases. However, the computation time increases as more particles are tracked. In this research, 200 particles were found to give a good balance between results variance and computation time.

From the nine geometries analyzed here, the pineapple 2D generates the highest distributive mixing capability. In general, the two pineapple mixers (1.6D and 2D) have the highest mean strains and the highest axial mixing, as shown with the cumulative residence time distribution. However, it is important to note that both pineapple mixers show the highest pressure and torque consumption.

The final distributive mixing capability in the experiments can be appreciated by qualitatively analyzing the micrographs in Fig. 7. For this analysis, a mix of a yellow master batch pigment and HDPE was used. The pineapple 1.6D mixer in Fig. 7(c) exhibits the thinnest striations and the rhomboid 1D3D (a) was found to develop the thickest. Because large strains are required to obtain small striations, the striation thickness in the micrographs can be compared to the strain calculated in the numerical analysis as shown in Table 2; here excellent agreement is found. The lighter circular region in the micrographs in Fig. 7 is an air bubble that appears after cooling the extrudate.

Although the design of the rhomboidal mixing section is intended for distributive mixing, it is interesting to evaluate the rhomboids dispersion capabilities. In general, the flow number indicates that

the nine geometries generate mainly shear flow. For good dispersion to occur a high flow number coupled with high stresses are desired. Therefore, none of the rhomboid mixers analyzed can be considered a good dispersive mixer.

4.4 Temperature Distribution

Figure 8 shows the average melt temperature profile measured by the thermal comb at 90 rpm for the three different die restrictions in the experiments. The temperature at the center is higher for all the mixers due to the heat generated by viscous dissipation, which is quantified in Table 3 by the mean bulk temperature (T_b). Due to the higher restriction imposed by the pineapple mixer, the material is subjected to a higher degree of viscous dissipation resulting in the highest T_b.

The melt temperature homogeneity can be quantified by looking at the maximum temperature difference and the standard deviation of the temperature measurements in Table 3. The rhomboid 1D3D is the mixer that results in the most homogeneous temperature profile and lowest viscous dissipation.

It is not necessary for the best distributive mixer to have the best temperature homogeneity. This effect is evident with the pineapple mixer. This mixer imposes the highest material deformation, but has the worst temperature homogeneity. Since the pineapple relies on higher residence times to impose more strain the material is also exposed to viscous dissipation for longer time.

The intention is not to compare the temperature results to simulations since the numerical results are computed assuming isothermal materials. The idea is to show that it is very difficult to find a mixer that can be the best distributive mixer and also the best temperature homogenizer. Generally, one has to find a compromise between the two variables or a combination of two mixers.

5 Conclusions

The tools used for this research demonstrated the usefulness of the BEM simulation for analyzing the rhomboidal mixing section. In this numerical study the rhomboid 2D-2D was predicted to have the highest distributive mixing capability, but at the same time it has the highest pressure consumption and torque demand. This result is in agreement with the experimental work performed.

For the operation range tested the rhomboid 1D4D was found to have the highest output. The nine geometries have a similar average flow number of approximately 0.5. In general, these mixers observe a shearing-type flow which is easiest to generate and is typical for most mixing sections.

It is very hard to decide on a mixer design that satisfies all the needs of the processor. The selection of the best mixer will depend on the desired mixing mechanism, and by balancing the mixing capability with the pressure consumption and torque requirements. The results suggest that the use of two mixers placed in series seems feasible. This solution is convenient when there is more than one quality to improve. To satisfy the mixing demands in industry, it is common to find two or more types of mixing devices in series in single screw extruders. It is easier to recommend an overall mixer combination in which the advantages and disadvantages of each mixing section compensate one another.

In this study a comparison was successfully done on the rhomboidal mixing section by numerically analyzing nine mixing geometries. Great insight was given on the flow phenomena that occur in these mixing systems. The numerical results compared very well with the three mixing sections analyzed experimentally.

Acknowledgements

The authors will like to thank the National Science Foundation under grant No. 9158145 and 3M for the financial support of this research. We acknowledge Multipath Corporation for providing the Fast Matrix Solver used for the simulations. All the experiments were performed at the Instituto de Capacitación e Investigación del Plástico y del Caucho (ICIPC) in Medellín, Colombia. Also, thanks are due to Plásticos del Lago C.A. from Venezuela y Dexton S.A. from Colombia who donated the PE-HD and PS-HI respectively and Concentrados Plásticos S.A. from Colombia for the master batches. Special thanks to Norberto Montoya who was patient enough to perform the micrographs and the material rheology tests.

References

[1] *Noriega, M.d.P.*: Paper presented at the PPS-European meeting, Stuttgart, Germany (1995)

[2] *Schumacher, F.*: Kunststoffe, 64, 6, p.274 (1974)

[3] *Daubenbüchel, W.*: Kunstsoffe German Plastics, 72, 5, p.290 (1982)

[4] *Müller, R., W. Michaeli, K. Hoffmann and T. Wolff*: Thesis, Institut für Kunststoffverarbeitung, Aachen, Germany (1997)

[5] *Michaeli, W., L. Czyborra and M. Heber*: Kunststoffe German Plastics, 81, 8, p.27 (1991)

[6] *Czyborra, L., and Michaeli, W.*: SPE Antec Tech. Papers 37, p.137 (1991)

[7] *Kalyon, D.M., A.D. Gotsis, Y. Ulku, C.G. Gogos, H. Sangani, B. Aral, C. Tsenoglou,*: Adv. Poly. Tech., 8, 4, p.337 (1988)

[8] *Meijer H. and H. Bos:* Einschneckenextruder – Grundlagen und System optimierung, p.25, June (1991)

[9] *Yao, C.-H. and Manas-Zloczower*: Int. Polym. Process, 7, 2, p. 92 (1997)

[10] *Kim, M.H. and J.L. White*: SPE Antec Tech. Papers 35, p.49 (1989)

[11] *Kiani, A.*: Paper presented at the Symposium on Numerical Simulation of Mixing Phenomena, AIChE annual meeting, November (1992)

[12] Fast Matrix Solver™ library from Multipath Corporation

[13] *Gramann, P.J., M.d.P. Noriega, A.C. Rios and T.A. Osswald*: SPE Antec Tech. Papers 43, p.3713 (1997)

[14] *Gramann, P.J. and T.A. Osswald*: Int.Poly.Process, p.303 (1992)

[15] *Davis, B.A., A.C. Rios, L. Stradins, and T.A. Osswald:* Paper presented at the Winter Annual Meeting of ASME, Chicago, (1994)

[16] *Rios, A.C., P.J. Gramann and T.A. Osswald*: Adv. Poly. Tech., 17, 2, p.107 (1998)

[17] Gramann, P.J., Ph.D. Thesis, University of Wisconsin, Madison, (1995)

[18] Lorentz, H.A., *Collected Works*, volume IV. Matrinus Nijhopff, Hague, (1937)

[19] Ladyzhenskaya, O.A., *The Mathematical Theory of Viscous Incompressible Flow*, Gordon and Breach, New York, (1963)

[20] *Ottino, J.M. and R. Chella*: Polym. Engr. Sci., 23, 7, p. 357 (1983)

[21] *Bigg, D.M.*: Polym. Engr. Sci., 15, 9, p. 684 (1975)

[22] *Oswald, T.A and G. Menges*: Materials Science of Polymers for Engineers, Hanser Publishers, Munich (1996)

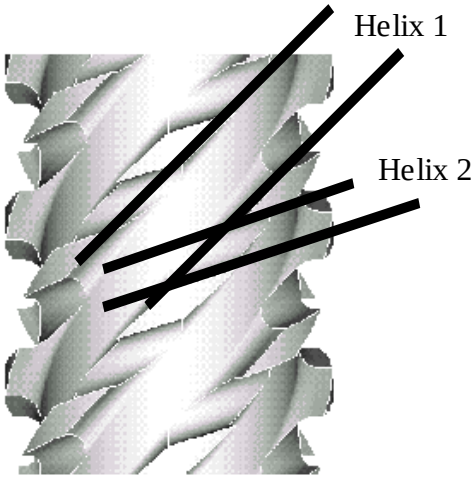

Figure 1. Geometrical parameters for designing rhomboidal mixing sections

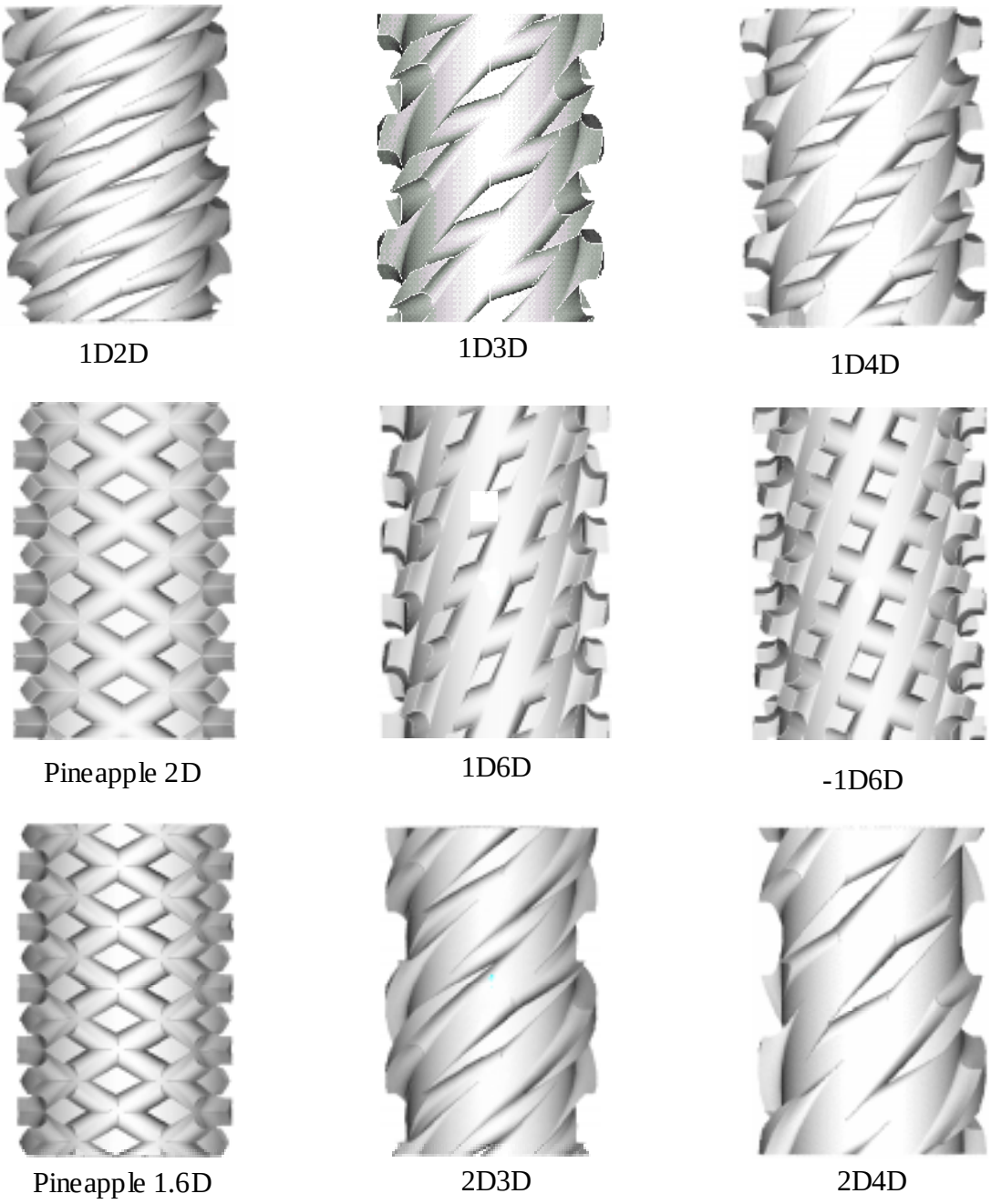

Figure 2. Geometries of rhomboidal mixing sections analyzed

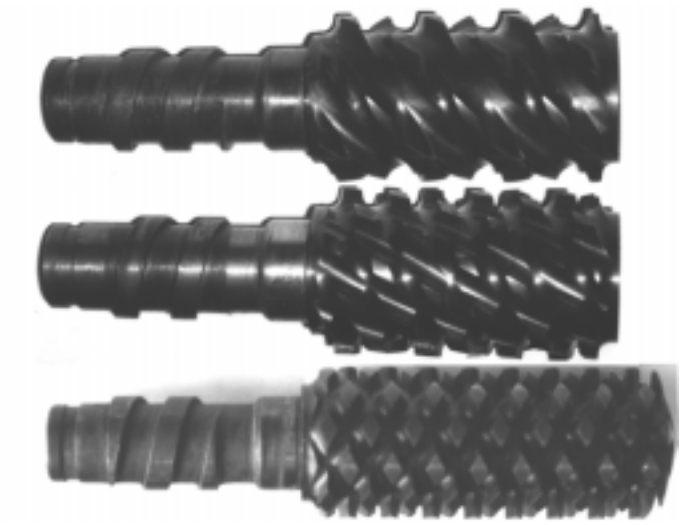

Figure 3. Picture of rhomboidal mixing sections studied in the experiments. From top to bottom: rhomboid 1D3D, rhomboid 1D6D and pineapple 1.6D

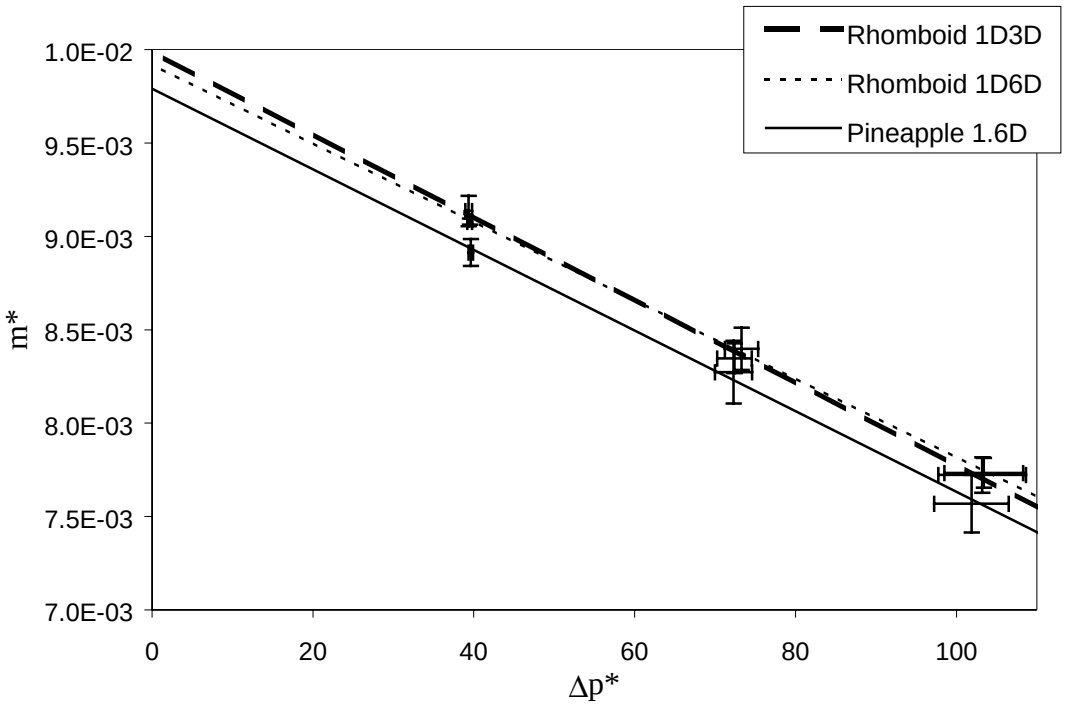

Figure 4. Experimental dimensionless screw characteristic curves for HDPE

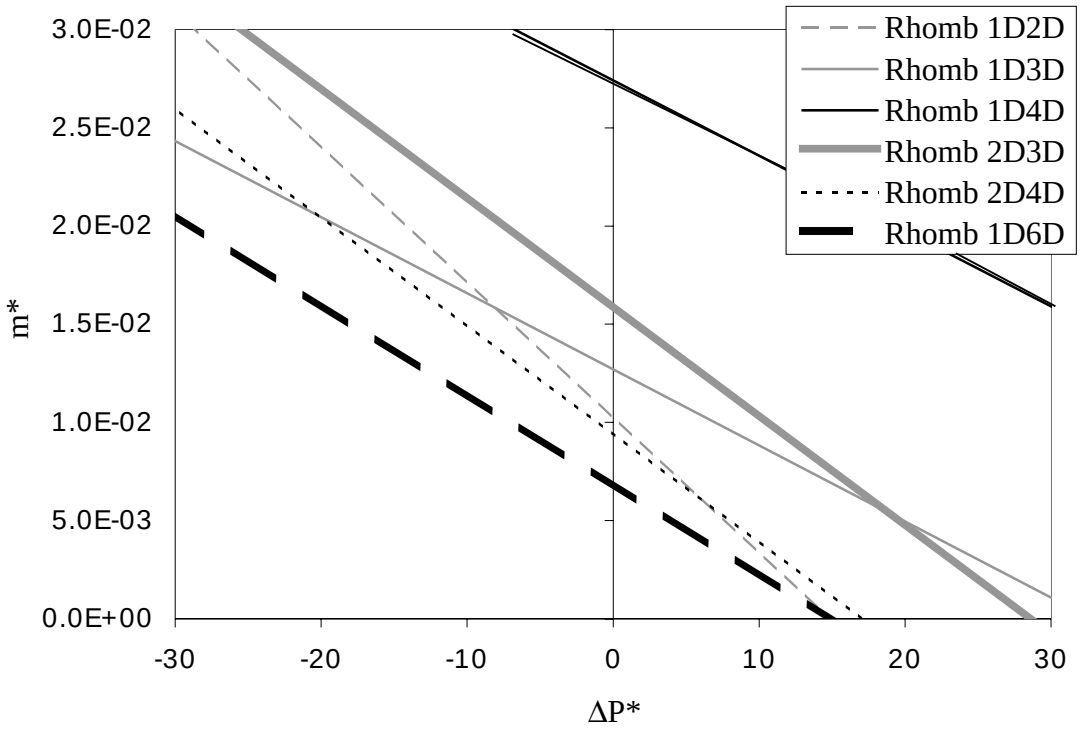

Figure 5(a). Characteristic curves of rhomboid mixing sections

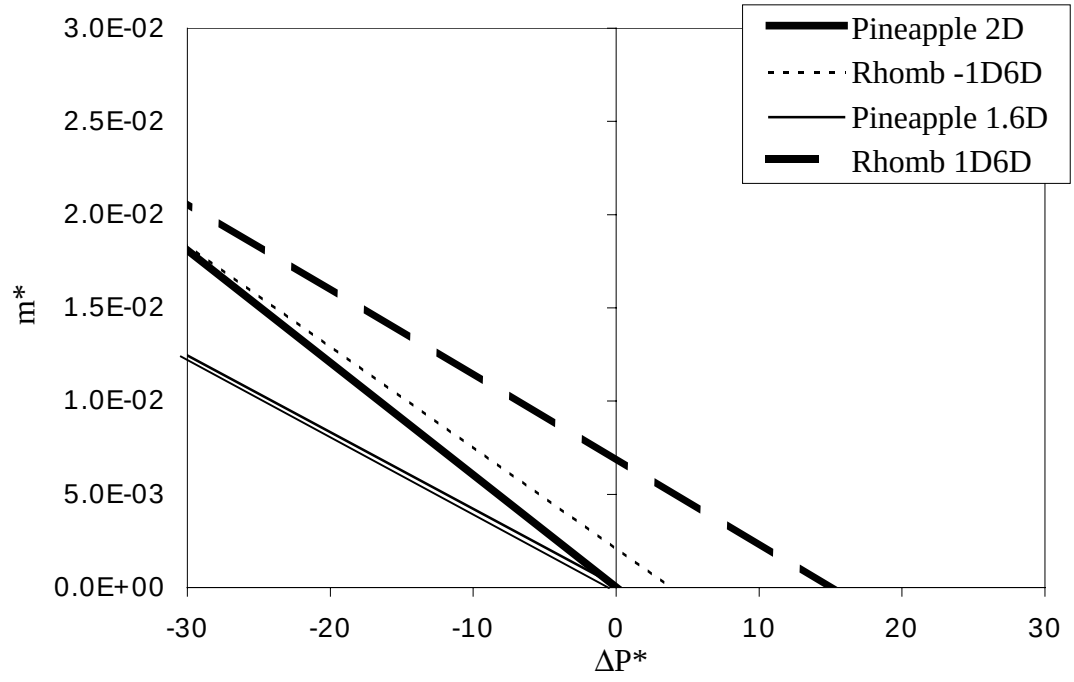

Figure 5(b). Characteristic curves of rhomboid mixing sections

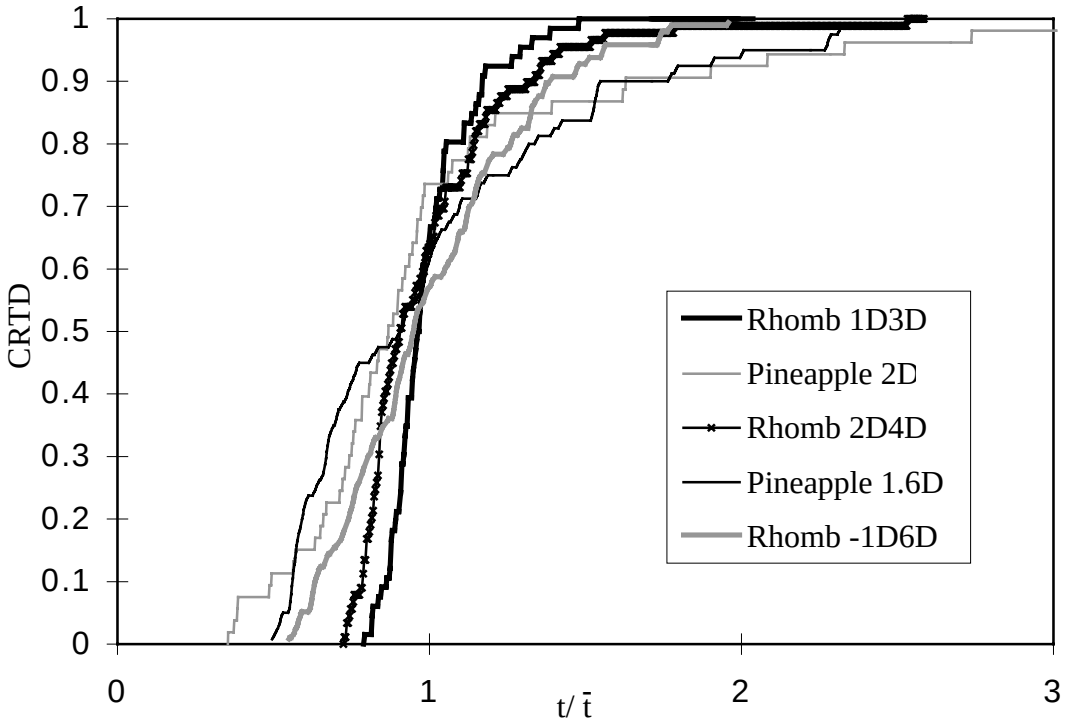

Figure 6. Residence time distribution of rhomboidal mixing sections

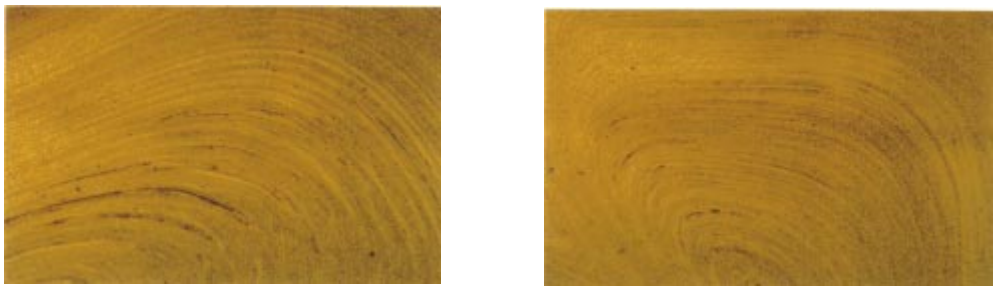

(a) (b)

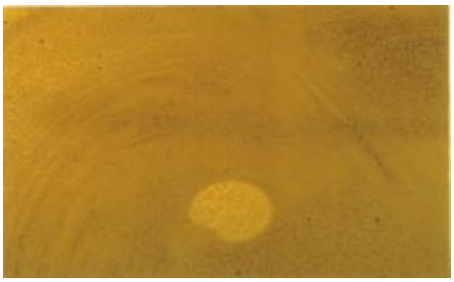

(c)

Figure 7. Extrudate micrographs (50x). (a) rhomboid 1D3D, (b) rhomboid 1D6D and (c) pineapple 1.6D

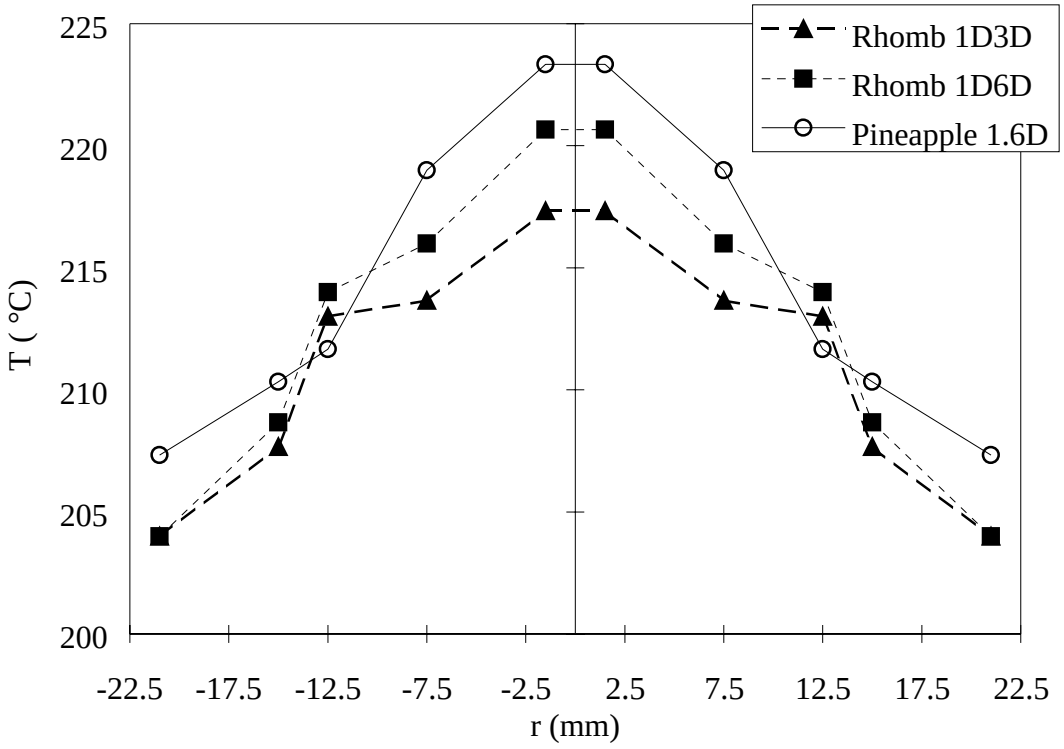

Figure 8. Average melt temperature profile at 90 rpm.

Table 1 Dimensions of rhomboidal mixing sections

Rhomboid	Pitch	Number of Cuts	Cut width (mm)
1D2D	1D	4	6.5
	2D	6	10.9
1D3D	1D	4	6.5
	3D	6	16.4
1D4D	1D	4	6.5
	4D	6	21.8
1D6D	1D	4	8.5
	6D	10	12.4
-1D6D	-1D	4	8.5
	6D	10	12.4
Pineapple 1.6D or	-1.6D	6	6.2
-1.6D1.6D	1.6D	6	6.2
Pineapple 2D or	-2D	6	8.0
-2D2D	2D	6	8.0
2D3D	2D	6	8.0
	3D	6	16.4
2D4D	2D	6	13.1
	4D	6	21.8

Table 2 Numerical results for nine rhomboidal mixing sections

Rhomboid	Torque (Nm)	Mean residence time, $\bar{t}$	Mean total strain	Flow no. λ	Mean strain Rate, $\lvert\dot{\gamma}\rvert$	β
1D2D	5.8	7.02	103.8	0.46	14.5	0.22
1D3D	6.1	5.88	80.7	0.46	13.6	0.15
1D4D	6.7	7.01	96.9	0.47	13.7	0.25
1D6D	7.3	6.94	109.2	0.47	15.5	0.25
-1D6D	7.7	9.73	126.0	0.48	12.4	0.33
Pineapple 1.6D	8.4	11.5	178.0	0.48	13.4	0.50
Pineapple 2D	8.3	20.71	218.2	0.49	11.1	0.49
2D3D	6.2	5.30	75.1	0.47	14.1	0.21
2D4D	6.6	5.03	72.0	0.47	14.2	0.26

Table 3 Temperature results at 90 rpm averaging the three different die restrictions

Mixing Section	T_b (°C)	σ^2 (%)	ΔT_{max} (°C)
Rhomboid 1D3D	207	2.4	13
Rhomboid 1D6D	208	2.9	17
Pineapple 1.6D	210	3.0	16